



Effects of Precursor Structure on First-Generation Photo-Oxidation Organic Aerosol Formation

D. Sofio, D. Long, T. Kohls, J. Kunz, M. Wentzel and D. Hanson*

Department of Chemistry, Augsburg University, Minneapolis, MN, United States

The effect of precursor molecular structural features on secondary organic aerosol (SOA) growth was investigated for a number of precursor functional groups. SOA yields were determined for straight chain alkanes, some oxygenated, up to highly functionalized hydrocarbons, the largest being β -caryophyllene. Organic SOA yield was determined by comparing to standard particle size changes with SO_2 in a photolytic flow reactor. SOA formation was initiated with OH radicals from HONO photolysis and continued with NO and NO_2 present at single-digit nmol/mol levels. Seed particles of ~ 10 nm diameter grew by condensation of SOA material and growth was monitored with a nanoparticle sizing system. Cyclic compounds dominate as the highest SOA yielding structural feature, followed by C-10 species with double bonds, with linear alkanes and isoprene most ineffective. Carbonyls led to significant increases in growth compared to the alkanes while alcohols, triple-bond compounds, aromatics, and epoxides were only slightly more effective than alkanes at producing SOA. When more than one double bond is present, or a double bond is present with another functional group as seen with 1, 2-epoxydec-9-ene, SOA yield is notably increased. Placement of the double bond is important as well with β -pinene having an SOA yield approximately 5 times that of α -pinene. In our photolytic flow reactor, first-generation oxidation products are presumed to be the primary species contributing to SOA thus the molecular structure of the precursor is determinant. We also conducted proton-transfer mass spectrometry measurements of α -pinene photooxidation and significant signals were observed at masses for multifunctional nitrates and possibly peroxy radicals. The mass spectrometer measurements were also used to estimate a HONO photolysis rate.

Keywords: organic compounds, secondary organic aerosol, structure, proton-transfer mass spectrometry, photo-oxidation

OPEN ACCESS

Edited by:

Yue Zhao,
Shanghai Jiao Tong University, China

Reviewed by:

Chaoyang Xue,
UMR7328 Laboratoire de physique et
chimie de l'environnement et de
l'Espace (LPC2E), France
Jianhui Ye,
Southern University of Science and
Technology, China

*Correspondence:

D. Hanson
hansondr@augsb.org

Specialty section:

This article was submitted to
Atmosphere and Climate,
a section of the journal
Frontiers in Environmental Science

Received: 09 March 2022

Accepted: 02 June 2022

Published: 24 June 2022

Citation:

Sofio D, Long D, Kohls T, Kunz J,
Wentzel M and Hanson D (2022)
Effects of Precursor Structure on First-
Generation Photo-Oxidation Organic
Aerosol Formation.
Front. Environ. Sci. 10:892389.
doi: 10.3389/fenvs.2022.892389

INTRODUCTION

It is well known that the oxidation products of gas-phase organic precursor compounds can adhere to aerosol particles, a process commonly referred to as the formation of secondary organic aerosol (SOA). Several review articles have presented their atmospheric prevalence, categorized laboratory results, and assessed mechanistic information (Kroll and Seinfeld, 2008; Jimenez et al., 2009). Particle size and composition are important determining factors of the role of aerosol (Zhu et al., 2017) in environmental and human health, on cloud formation and on the Earth-Sun radiative balance (Haywood and Boucher, 2000; Tuet et al., 2017; Praske et al., 2018; Lee et al., 2019).

The structural features of the precursor organic molecules are known to affect the amount of SOA formed (Keywood et al., 2004; Raventos-Duran et al., 2010; Lee et al., 2006a; Lee et al., 2006b), for example cyclic alkane structures are more active than linear ones with branched alkanes the least active (Lim and Ziemann 2009; Tkacik et al., 2012; Hunter et al., 2014). Hunter et al. (2014) discussed a tethering effect for the multifunctional products form in the oxidation of ring structures. Studies have also related the number of double bonds in a compound to its SOA behavior (Ng et al., 2006) and to the rate of H-shift reactions once photo-oxidized (Møller et al., 2020); our previous experimental work (Hanson et al., 2022) with a series of monoterpenes is consistent with these ideas. Other studies have looked in great detail at a few molecules that are structurally similar and found differences in SOA yields (Sato et al., 2012; Chiappini et al., 2019).

Here we add to the knowledge of SOA formation by exploring its dependence on precursor structure at low amounts of organic aerosol. A study of a large suite of molecules with a focus on the very low volatility, first-generation SOA capabilities (i.e. low exposures of products to OH; there can be multiple NO molecules taking part) may help tie together some of these ideas regarding precursor functionality and structure.

We determine the effect of structural features and functional groups of a precursor compound by comparing the relative SOA yields calculated on a mole basis. Our goal is to determine the effects of functional groups and the structure of the precursor molecules on the growth of ~10 nm diameter sulfuric acid seed particles without the influence of multi-generation photooxidation products. We examined straight-chain alkanes, octane through dodecane, and then C9 and C10 alkanes with carbonyls, double bonds, triple bonds, and cyclization among other structural features. We discuss our results in the context of previous studies with a focus on first-generation results.

A set of measurements with a proton-transfer mass spectrometer are presented that show a suite of product ions in the photo-oxidation of α -pinene. In a model-measurement comparison to assess the photolysis conditions, the HONO photolysis rate was determined from the measured loss of α -pinene.

MATERIALS AND METHODS

Experiment. Photo-oxidation experiments on alkanes, alkenes, alkynes, cyclic compounds, carbonyls and an alcohol were performed in a growth photolytic flow reactor, GroFR. The GroFR apparatus and methodology has been described in detail (Hanson et al., 2022) and here an overview of the technique is presented.

GroFR consists of a 125 cm long, 5 cm inner diameter, glass flow reactor with several ports where up to eight flows (purified air, AADCO 737) were added. Flows entering at the top of the reactor add up to 1.5 standard (273 K, 1 atm) L/min. These are: a humidified flow, a dry flow, a sulfuric acid (SA) aerosol flow, a HONO-laden (~10 $\mu\text{mol/mol}$, ppmv, in air) flow designated Q_4 , and a flow containing either an organic or SO_2 . Relative humidity was constant at 35%, a circulating fluid maintained a

flow reactor temperature of 23 °C (296 K) and pressure was typically 0.98 atm. Photolysis of nitrous acid at ~370 nm (UV LEDs: ~90% emission between 350–380 nm) initiated photo-oxidation and oxidation rate was varied primarily by changing Q_4 , the flow rate of the HONO-laden air. HONO was generated by reacting HCl gas with sodium nitrite (Febo et al., 1995; Gingerysty and Osthoff, 2020). NO impurity levels were about 2–3% of HONO, determined with a TECO 14B/E; for most of the measurements initial NO was 0.8 to 1.3 nmol/mol (ppbv) but was up to 4.5 ppbv at the highest Q_4 . Typical residence time was 85 s but with laminar flow established over most of the reactor (supplement S2 of Hanson et al., 2022), the on-axis residence time is about half of that. Typical [OH] is $1 \times 10^7 \text{ cm}^{-3}$ (as modeled in Hanson et al., 2022) but for low vapor pressure compounds, OH levels can rise to ten times this and OH reaction with HONO becomes significant. For typical conditions, less than 1% of first-generation products react further with an OH molecule.

An aliquot of an organic compound of interest (approximately 1 ml) was placed in a vessel and a small air flow (0.5 to 5 sccm: standard cm^3/min) became saturated and entered the reactor. For high volatility compounds the vessel was submerged in an ice bath. See the **Supplementary Material** for information on the vapor pressures of the compounds studied here, their estimated levels in the flow reactor, and their sources and purities.

Seed particles are roughly 50 wt% sulfuric acid particles of ~9 nm diameter present at number densities of 200–1,000 cm^{-3} in the reactor. Their initial sizes and their growth upon photo-oxidation of the organic compound were observed with a nanoparticle mobility sizing system (diethylene glycol as detector working fluid, Jiang et al., 2011). The measured changes in diameter, ΔD_p , were examined as a function of Q_4 which is proportional to the initial level of HONO. Consistent with our previous work, the present experimental results show that there is generally a direct linear relationship between ΔD_p and Q_4 .

Using small particles avoids significant gas-phase diffusion limitations to the uptake of gaseous species. Their composition is believed to be primarily sulfuric acid and water which is an atmospherically relevant particle type. Our experimental conditions differ from the majority of SOA experiments where seed particles are ammonium sulfate (or bi-sulfate), oxidation is carried out for long time periods and the mass concentration of organic material is large (the present experiment has organic aerosol concentration at a maximum of about 0.005 $\mu\text{g}/\text{m}^3$). Comparisons with previous work are complicated for all of those differences but acid-catalyzed reactions are a special concern. We argue below (as we have previously, Hanson et al., 2022) that acid-catalyzed reactions are not the dominant factor driving SOA in our measurements. We also present measurements in the Supplement that support this viewpoint where α -pinene SOA was found to be nearly independent of relative humidity and thus acid activity: less than a 20% fluctuation in ΔD_p measured over the range of 17–70% RH.

Our experimental SOA yields are based on a comparison to growth measurements with H_2SO_4 molecules. The slope of a

regression line for the ΔD_p vs Q_4 (directly proportional to [HONO]) can be related to an SOA yield by comparing to slopes of data from SO_2 photo-oxidation experiments; differences in their photo-oxidation are accounted for. The following section presents an overview of the analysis; full details of the comparison and yield determination are presented in Hanson et al. (2022).

Quantifying SOA yield. The SOA yields are calculated on a mole basis, Y_{mol} ; a mass-based SOA yield, Y_{mass} , as used in many studies, can be calculated from the mole-based SOA yield by multiplying by the molar mass ratio of the assumed SOA species, MM_{SOA} , to that of the precursor (MM_{HC}):

$$Y_{\text{mass}} = \frac{MM_{\text{SOA}}}{MM_{\text{HC}}} Y_{\text{mol}}$$

Differences in SOA density (here, 1.2 g cm^{-3}) used for the yield calculations need to be considered also.

Yields can be calculated from a diameter growth rate equation along with a kinetic model if the oxidation chemistry can be suitably simplified, as done by Krasnomowitz et al. (2019) for α -pinene ozonolysis yields. Here, we do use a diameter growth rate equation but the yields are placed on an absolute basis by standardizing to growth observed in photo-oxidation of SO_2 experiments where the product H_2SO_4 is formed at 100% yield. Differences in experimental conditions and the molecular properties that go into the growth rate are taken into account: fluence; the particle molar volumes of sulfuric acid and of the oxidized organic species (an assumed SOA “molecule”); diffusivities and mean thermal speeds (kinetics); the regeneration of OH (a chain length, primarily from $\text{HO}_2 + \text{NO}$) must be calculated.

Equation 1 details how these considerations contribute to Y_{mol} in a series of factors: gas-phase kinetic processes (f_{kin}), particle-phase volumes (f_{vol}), and differences in OH-regeneration between the organic and the SO_2 experiments (f_{CL}). F is the product of these factors and it takes values of 2.2 for 10 carbon precursors, ranging from 1.5 for 15 carbon precursors to 2.7 for eight carbon precursors. Equations (1a)–(1e) are discussed in reverse order in the following paragraphs.

$$f_{\text{kin}} = \frac{k_{\text{SOA}}^{\text{I}}}{k_{\text{SA}}^{\text{I}}} \frac{c_{\text{SA}}^{\text{P}}}{c_{\text{SOA}}^{\text{P}}} = \frac{D_{\text{SOA}}}{D_{\text{SA}}} \frac{c_{\text{SA}}^{\text{P}}}{c_{\text{SOA}}^{\text{P}}} \quad 1(a)$$

$$f_{\text{vol}} = \frac{V_{\text{SA}}}{V_{\text{SOA}}} \quad 1(b)$$

$$f_{\text{CL}} = \frac{\Delta \text{SO}_2}{\Delta \text{Org}} \quad 1(c)$$

$$F = f_{\text{kin}} f_{\text{vol}} f_{\text{CL}} \quad 1(d)$$

$$Y_{\text{mol}} = F \frac{m_{\text{org}}}{m_{\text{SO}_2}} \frac{I_{\text{SO}_2}}{I_{\text{org}}} \quad 1(e)$$

The m_{SO_2} and m_{org} are the slopes of the diameter change ΔD_p vs Q_4 data. The last term in Eq. 1(e) is the ratio of LED currents for the SO_2 , I_{SO_2} , and the organic, I_{org} , experiments.

Particle growth is effective in the SO_2 experiments therefore the current through the LED strings was reduced to 0.2 A; the organic experiments were conducted at full illumination, a current of 2 A

through the LED strings. This current is proportional to fluence and thus it directly affects the HONO photolysis rate: growth was shown to be proportional to this current (Hanson et al., 2022).

The chain length factor f_{CL} is essentially how many SO_2 molecules are lost divided by how many organic molecules are lost per HONO molecule photolyzed. It was evaluated with the 2 dimensional model (Hanson et al., 2022) of the flow reactor where loss of SO_2 was compared to the loss of a prototypical organic, in this case α -pinene. We assume no significant change in f_{CL} with the type of organic. This was substantiated by running a cyclohexane photo-oxidation scheme and a comparable value for f_{CL} was obtained (Hanson et al., 2022). Calculating changes in f_{CL} with type of organic is not worthwhile at this time in part because of unknown and/or uncertain oxidation schemes.

The factor f_{vol} is the ratio of the particle-phase molar volume of sulfuric acid V_{SA} divided by V_{SOA} , an estimated molar volume of SOA material. We assume a molar volume for putative SOA material, V_{SOA} in f_{vol} , Eq. (1b), that scales with the number of carbons of the precursor, retains all hydrogens, and has an O:C ratio of 0.5. Thus V_{SOA} was calculated from MM_{SOA} that is about 1.6 times the precursor molar mass and an assumed density of 1.2 g/cm^3 .

The kinetic factor f_{kin} contains the gas-phase species x 's first-order loss rate coefficient (k_x^{I}) and the mean thermal speed of the particle- x encounter (c_x^{P}). $k_{\text{SOA}}^{\text{I}}$ can vary quite a lot depending on what first-order loss process is dominant for the SOA “molecule”. For example, a peroxy radical's main loss is reaction with NO which gives a $k_{\text{SOA}}^{\text{I}}$ on the order of 0.5 s^{-1} for typical conditions. Stable species that do not stick to the wall have a $k_{\text{SOA}}^{\text{I}} = 0.012 \text{ s}^{-1}$, the inverse of the residence time.

For $k_{\text{SOA}}^{\text{I}}$ we assume these first-generation SOA “molecules” stick to the wall efficiently as well as to the seed particles. Also we assume their first-order loss is dominated by diffusion to the wall governed by its diffusion coefficient, D_{SOA} . For H_2SO_4 this is a certainty and its diffusion coefficient is D_{SA} (Hanson and Eisele, 2000) and k_{SA}^{I} is $\sim 0.045 \text{ s}^{-1}$ for the conditions of this study. With these assumptions, the kinetic factor f_{kin} takes a value of about 0.9 and it does not change significantly with the type of precursor: species diffuse more slowly as they get heavier and larger but their collision rates with particles decreases concomitantly. If the SOA is due to uptake of peroxy radicals, this assessment of f_{kin} is not valid: f_{kin} can be much larger in this case. Furthermore, the yield of peroxy radicals in photo-oxidation of organic compounds is 100% (or more) so that Y_{mol} in this context is complicated and folds in heterogeneous chemistry parameters (Hanson et al., 2022).

For additional details regarding the diameter growth rate kinetic equation and the meaning, derivation, and parameters in the formulas in Eq. 1, see Hanson et al. (2022). Note that the quantities in Eq. 1 are relatively well-known for H_2SO_4 formed from SO_2 photo-oxidation in our reactor.

Comparison to partitioning ideas. Our analysis presumes growth occurs by essentially involatile species. A partitioning model, such as the volatility basis set model (Donahue et al., 2011), may not be helpful for analyzing our experimental results because wall loss can be dominant and the amount of aerosol mass is very low: a maximum organic loading of $\sim 0.005 \text{ } \mu\text{g/m}^3$. In this model a compound partitions to the condensed phase at 10% if its saturation pressure is $6 \times 10^{-12} \text{ atm}$ ($0.05 \text{ } \mu\text{g/m}^3$ for a molar

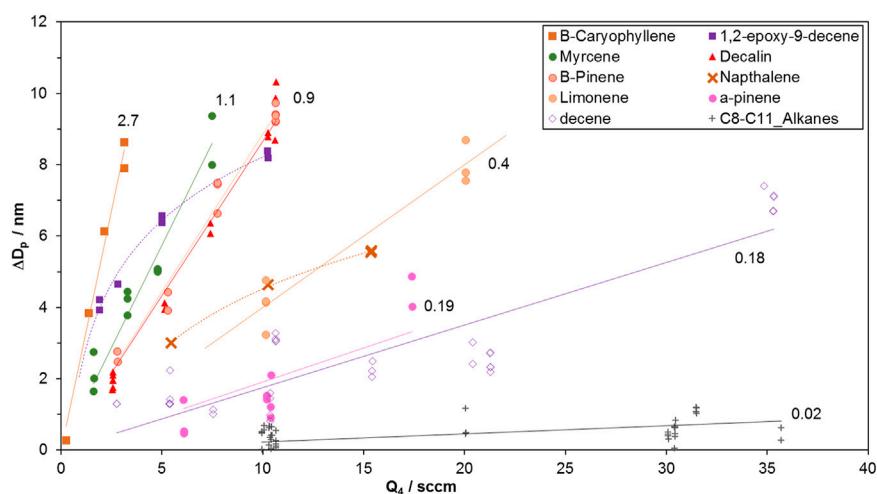


FIGURE 1 | Growth vs HONO-laden flow of clean air, Q_4 (HONO is present at ~ 10 ppmv in this flow). At $Q_4 = 10$ sccm, the initial HONO abundance in the flow reactor is 64 ppbv or $1.5 \times 10^{12} \text{ cm}^{-3}$, taking into account the initial NO and NO_2 impurities, each at $\sim 2\%$. Slopes (nm/sccm) are indicated next to the regressions lines (forced through zero.). Note the non-linear data for 1,2-epoxydec-9-ene and naphthalene where the curvature indicates larger yields at lower oxidation rates. The abundance of these species in the flow reactor may have been low: epoxydecene's vapor pressure is unknown and is estimated to be low and naphthalene loss onto the delivery lines was an issue. At low precursor abundances, OH radicals can significantly react with HONO, potentially limiting the amount of SOA formed. The SOA yields for these two species were taken from the initial change in diameter, i.e. $\Delta D_p/Q_4$ at the lowest Q_4 value. β -caryophyllene and the C-12 species also have low vapor pressures. The data is clearly linear for β -caryophyllene which is not unexpected at the low HONO for these experiments (see **Supplementary Material** for more discussion). SOA formed from the C-12 precursors was low (average ΔD_p over all Q_4 was less than 1 nm) yet the data was noticeably not linear; the lower limit yields were taken from $\Delta D_p/Q_4$ at the lowest Q_4 .

mass of 220 g/mol). Yet if the steady-state partial pressure of a species greatly exceeds this vapor pressure it can be considered involatile and particles will grow.

Growth in our experiment is driven by whether a species steady-state concentration sufficiently exceeds its vapor pressure. For example, suppose a species has a vapor pressure of 6×10^{-12} atm and that it is produced at $Y_{\text{mol}} = 4\%$ (its gas-phase yield during putative first-generation photo-oxidation of an organic). Assuming steady-state is established in the second half of the flow reactor, this species will attain a partial pressure of 1.3×10^{-10} atm at $Q_4 = 10$ sccm, particles grow by about 2 nm, and there are about 2×10^6 per cm^{-3} of this species on particles. This is a partitioning to the particle phase of only about 0.001.

Mass spectrometer. A proton-transfer mass spectrometer (Hanson et al., 2009) sampled the middle of the flow through a 1 m length of 1/8" OD Teflon tubing. The sampling tube and the ion drift region were at room temperature. Drift tube E/N settings were ~ 120 Td with an electric field of 310 V/cm at a gas density n of $2.6 \times 10^{17} \text{ cm}^{-3}$ ($1 \text{ Td} = 1 \text{ V cm}^{-1} 10^{17} \text{ cm}^{-3}/n$) and ~ 70 Td at an electric field $E = 180$ V/cm and the same n . At low E/N, there is little breakup of ions such as the $M-H^+$ parents of α -pinene and pinonaldehyde. Also at low E/N, there are observable signals for a number of compounds with masses between 200 and 270 u. Both E/N settings were used to measure α -pinene loss for the estimation of the photolysis rate of HONO.

RESULTS AND DISCUSSION

The measured change in particle diameter were plotted against HONO level and fitted with linear regressions forced through the

origin; a linear relationship encapsulated the growth for most of the compounds, within the scatter of the data. **Figure 1** shows representative data for many of the compounds investigated here.

The slopes of the regression lines for all the compounds investigated are presented in **Table 1**. These slopes were used to calculate SOA yields Y_{mol} from Eq. 1 with the values of F listed in the table and $I_{\text{SO}_2}/I_{\text{org}} = 0.10$. Because the scatter in the data is large, a few species with slopes within ten % of each other were grouped in a single row in the table.

β -Caryophyllene and 1,2-epoxydec-9-ene are most effective with a lower limit to the SOA yield for both of 40%. Next is myrcene at 24% followed by decalin and β -pinene with SOA yields of 20%. Reasonably effective SOA producers are naphthalene at 11%, limonene at 10%, and α -pinene and 1-decene at about 4%. Of the straight chain species without a double bond, the carbonyls, an alcohol, and the C12-species resulted in the highest SOA yields of 1–1.5%. Isoprene, smaller alkanes and other functional groups were also not effective producers of SOA in our experiment. These functional groups included a triple bond, and an aromatic (1-decyne and 1,3,5-trimethylbenzene, respectively). The previous results from our system for α -pinene and limonene (Hanson et al., 2022) agree well with the present measurements, 4 and 8.4%, respectively, but our previous 16% yield for myrcene is 33% lower than the present results. A detailed comparison of SOA yields for these three monoterpenes is presented in Hanson et al. (2022). The comparison of the results with previous work for several of the other compounds is discussed below.

The photo-oxidation results of both of β -caryophyllene and 1,2-epoxydec-9-ene show large and comparable effects on particle

TABLE 1 | SOA Yields for Organic Compounds Examined in GroFR. All species in the last six rows are straight chains except for trimethylbenzene and isoprene. Density of the SOA was assumed to be 1.2 g cm^{-3} for all species and molar mass was assumed to have an O:C ratio of 0.5.

Compound	Slope, Nm/Scm	F	Y_{mol} (%)
β -caryophyllene ^a	2.7	1.5	40
1,2-epoxydec-9-ene ^a	1.8	2.2	40
myrcene	1.1	2.2	24
decalin, β -pinene	0.9	2.2	20
naphthalene ^a	0.5	2.2	11
limonene	0.44	2.2	10
α -pinene, 1-decene	0.19, 0.18	2.2, 2.2	4
1-nonanal, 1-decanal, dodecane ^a	0.07	2.4, 2.2, 1.8	1.7, 1.5, 1.3
2-nonanone, 1,2-epoxydodecane ^a	0.05	2.4, 1.8	1.2, 0.9
decane, 1-decyne, octanol	0.04	2.2, 2.2, 2.7	0.8, 0.8, 1.1
nonane, 1,3,5-trimethylbenzene	0.02	2.4	0.5
undecane, octane	0.02	2.0, 2.7	0.4, 0.5
isoprene	0.01	4.4	0.4

^aLow vapor pressure species and, for naphthalene, delivery issues; yields are lower limits.

growth despite large differences in precursor structure. The former is bicyclic, has two double bonds while the latter is linear with a single double bond. A significant branch in β -caryophyllene photo-oxidation pathway involves ring opening which can lead to bidentate oxygenated moieties. The epoxydecene species can also lead to oxygenated moieties on both of its ends if an efficient H-shift reaction occurs between the initial hydroxy-peroxy radical and an H atom on or near the epoxide carbons (the initial radical being formed upon OH addition to the double bond then O_2 onto the radical site.) The SOA material here being characterized by two oxygenated regions of the molecule that are widely spaced. Previous work with β -caryophyllene photo-oxidation where early yields could be determined (Ng et al., 2006; Alfarra et al., 2012; Tasoglou and Pandis, 2015) show a range of $Y_{\text{mol}} = 16\text{--}25\%$ (using $1.6 \times 204 \text{ g/mol}$ for MM_{SOA} and their 25–40% mass-based SOA yields); their overall yields at long times were larger. Chan et al. (2011) showed that the sulfate aerosol-phase products of β -caryophyllene ozonolysis depended on acidity however this may not affect the SOA yield because it was not clear if other gas-phase species were taken up. Kroll and Seinfeld (2008) summarize the ambiguity of the effect of acidity in previous work. In our previous work (Hanson et al., 2022) we presented arguments that aerosol-phase reactions such as oligomerization, that may be acid catalyzed, are not dominant in our experiments. See the **Supplementary Material** also for measurements of Y_{mol} for α -pinene that showed little dependence on relative humidity. Finally, we note that the diameter of particles that were nucleated (see below) are comparable to the change in diameter of the sulfuric acid seed particles, suggesting that acid is not necessary for SOA in our experiments.

It is clear that cyclic compounds and that most species with multiple double bonds or a double bond and another functional group lead to oxidized molecules that are taken up effectively onto the seed particles. Our decalin Y_{mol} of 20% is comparable to that reported by Li et al. (2019) at their lowest OH exposure ($[\text{OH}] \times t = 1.5 \times 10^{11} \text{ cm}^{-3} \text{ s}$, about 100 times that of this work) of $Y_{\text{mol}} = 14\%$ (22% mass-based, using $\text{M}_{\text{SOA}} = 1.6 \times \text{MM}_{\text{decalin}}$).

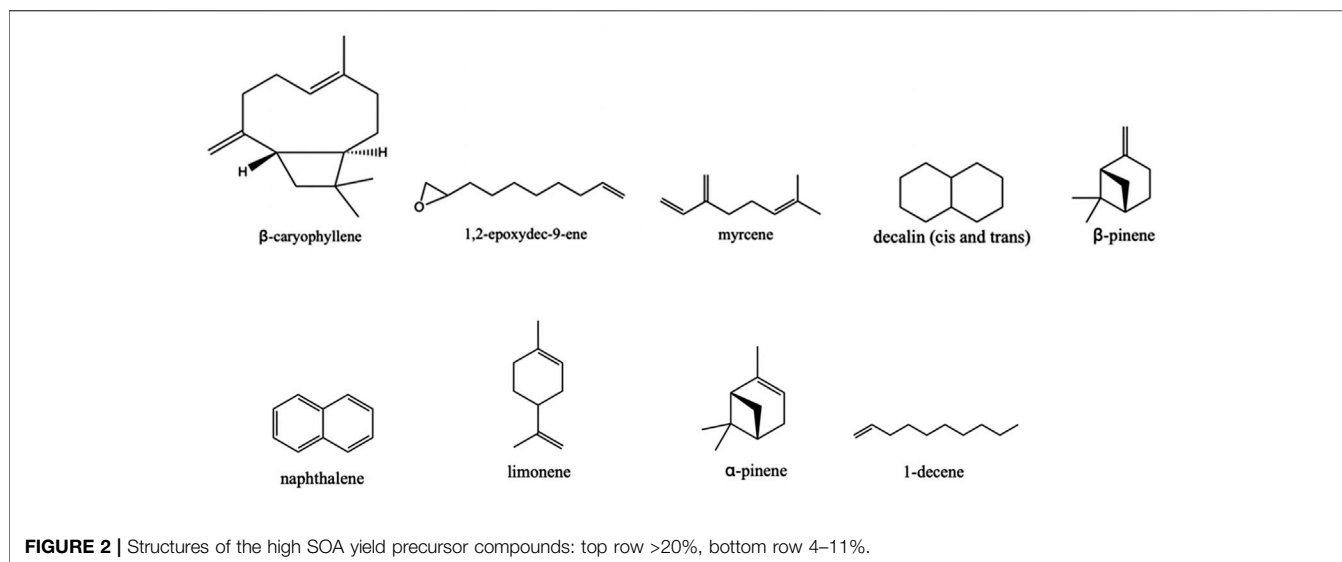
Our results show that β -pinene is effective at producing SOA, comparable to the capabilities of decalin and of myrcene (no rings,

three double bonds) and about 5 times better than α -pinene. Previous experimental results for initial Y_{mol} from Ng et al. (2006) and Zhao et al. (2015) are roughly 7 and 4%, respectively, from their mass based yields of 11 and 6.8%; which are substantially lower than the present $Y_{\text{mol}} = 20\%$. Yet these studies are consistent with the present results in that SOA yields are a factor of 2–3 higher for β -pinene than for α -pinene. Support in the literature for this trend is mixed. Theoretical branching ratios (Vereecken and Peeters, 2012) for these channels suggest there is a factor of 2.6 larger production of ring-opened peroxies from β -pinene over that for α -pinene. On the other hand, recent experiments indicate that larger amounts of highly-oxidized molecules arise from α -pinene OH reactions than from β -pinene OH reactions (Berndt et al., 2016). This is echoed in the α -pinene and β -pinene branching ratios for the ring-opened peroxy radicals reported by Xu et al. (2019) (larger branching for α -pinene than for β -pinene).

Naphthalene has been previously investigated (Chan et al., 2009) and their growth curves indicate that initial mass-based SOA yields were on the order of 10 and ~50% for high and low NO_x conditions, respectively. Our lower limit of ~11% mole-based yield lies between these two results; further comparisons are not warranted because of differences in experimental conditions. Our measurements suffered from purported surface effects due to interactions of naphthalene with glass surfaces and the Teflon lines delivery system. After these experiments were done, the tubing was replaced and the glass trap was put in an oven with clean gas flowing to degas it overnight.

Trimethylbenzene and isoprene were particularly inefficient in forming SOA material for the conditions of this experiment. These findings are consistent with the trimethylbenzene results of Li et al. (2021) and the initial isoprene SOA formation curves of Ng et al. (2006).

The effect of other functional groups can be seen in the results for the straight chain C-10 compounds. SOA yield increases from low values for decane and decyne, to a SOA yield roughly double that for decanal, to a roughly 5 times yield for 1-decene, to a roughly 50-fold increase for 1-epoxy-9-decene. The double bond on the decane backbone has the most effect and an epoxide along with it is very effective.



Our measurements indicate carbon-chain length has an influence on SOA yield, despite the difficulties in determining these low SOA yields (1%). The decane and dodecane yields of 0.8 and 1.1% are higher than the ~0.4-to-0.5% yields for octane, nonane and undecane. Nonetheless, all the alkanes presented here have low SOA yields, and are not effective at growing particles following oxidative photolysis for first-generation products. Previous work report much larger yields for decane, 10–25% mass-based (Lim and Ziemann, 2009; Hunter et al., 2014): the much larger aerosol loadings and longer oxidation times of the previous work are probably responsible for the differences in yields with the present work.

The high SOA yielding molecules are 1) bi-cyclic or 2) they have a double bond and another functionality. The bi-cyclics include β -caryophyllene, decalin, β -pinene and naphthalene all with yields >10%. Notably, decalin and naphthalene are absent of other functional groups and this highlights the SOA forming capabilities of the ring-opening oxidation pathway (Lim and Ziemann, 2009) that leads to two oxygenated moieties. Further oxidation of decalin by another OH molecule may open the other ring and contribute to the high yields found for large OH exposures (Hunter et al., 2014; Li et al., 2019). The second group of high SOA yield compounds includes epoxydecene, myrcene, and limonene that have at least one double bond and a second functionality. These species are probably susceptible to fast H-shift reactions (Vereecken and Nozière, 2020) involving the peroxy radical formed after initial OH-addition to the double bond (limonene more so with the ring-opening of this compound after reaction with NO occurs). These H-shift reactions leave widely separated oxygenated moieties that can enhance uptake onto the seed particles. The propensity to form widely separated oxidized carbon atoms seems to be a unifying explanation for the SOA activity of an organic compound.

We have postulated that a direct uptake of peroxy radicals onto the seed particles can play a role in α -pinene photo-oxidation (Hanson et al., 2022). A peroxy radical can be

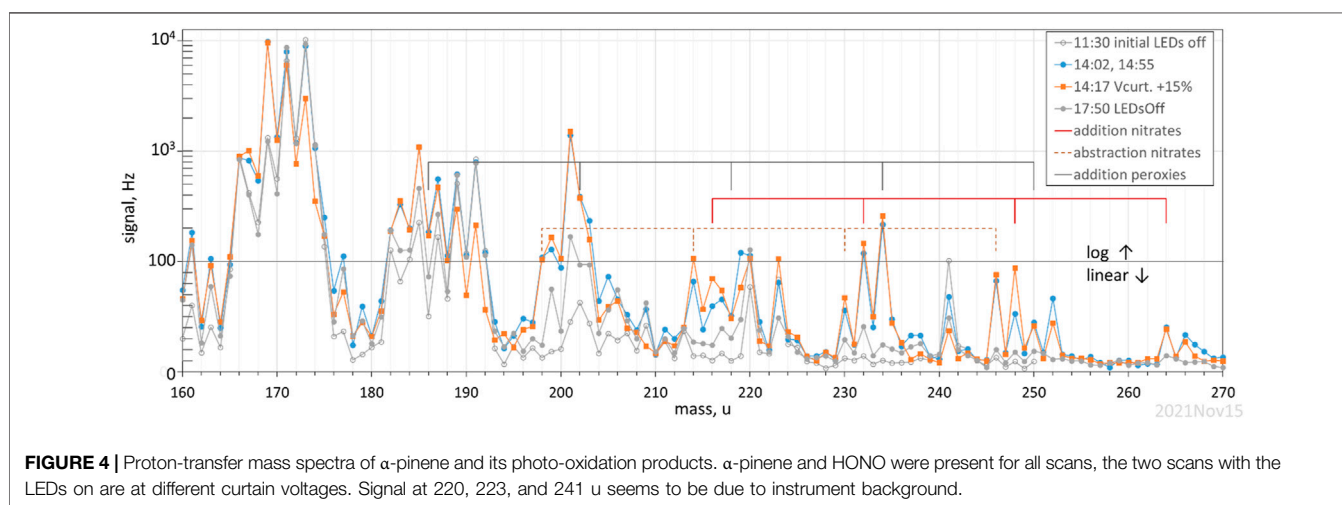
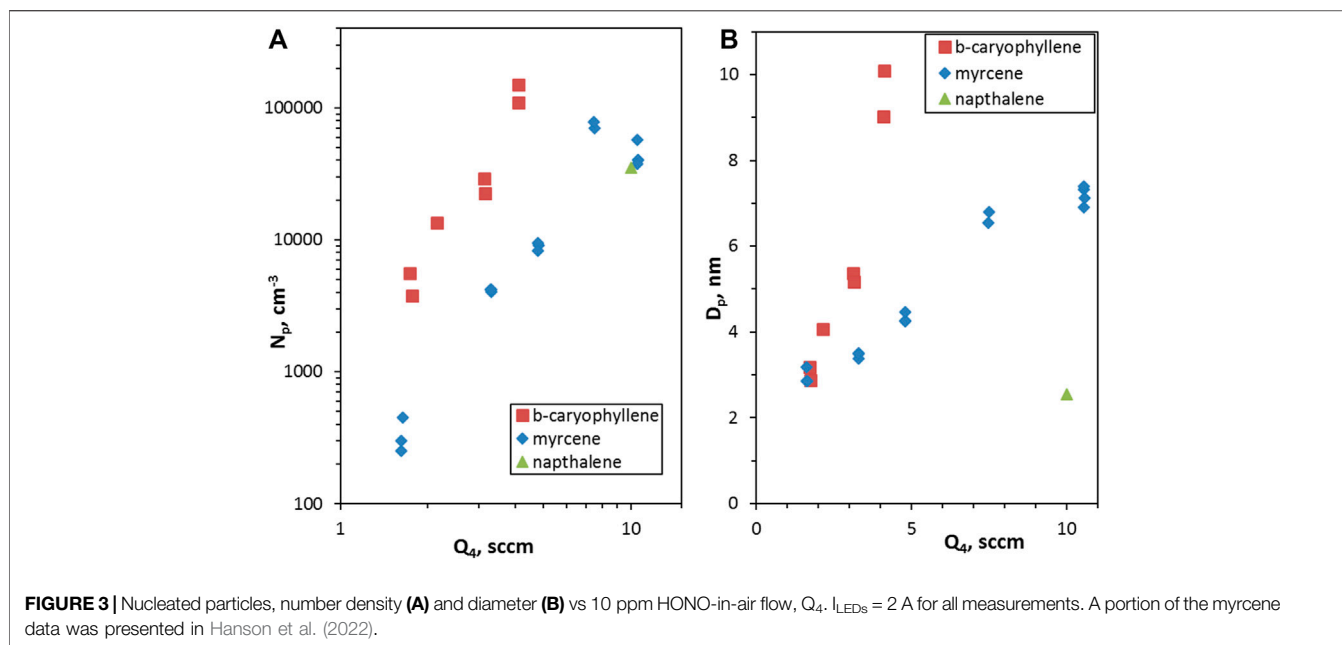
present in both the high-yield groups, 1) and 2), however, the Y_{mol} of these high-yield groups is not necessarily due to uptake of peroxy radicals due to self-reaction: the rough estimate for this type of process for the α -pinene peroxy radical gave a putative Y_{mol} of ~0.03.

The lowest SOA yield compounds shown in **Figure 2** are α -pinene and decene with yields of about 4%. The placing of the double bond in the ring mutes the ring opening channel for α -pinene (Vereecken et al., 2007) below that for β -pinene. The ring-opening channel peroxy radical is believed to undergo significant rates of H-shift, leading to R(OH)(OOH) O_2 radicals. The initial hydroxy-peroxy radical formed from decene reacts primarily with NO in our experiment leaving a hydroxy-alkoxy radical, a fraction of which may undergo an H-shift, add O_2 , and produce R(OH)(OH) O_2 radicals. These multifunctional peroxy radicals may undergo heterogeneous chemistry that might be a significant component of the observed particle growth.

Nucleation

Photo-oxidation of three of the compounds resulted in significant formation of new particles in addition to growth of the seed particles: β -caryophyllene, myrcene, and naphthalene. Shown in **Figure 3** are the number of particles produced 1) and the leading edge diameter 2). Many previous studies have noted nucleation from photo-oxidation of β -caryophyllene (Lee et al., 2006b; Ng et al., 2006; Alfarra et al., 2012; Tasoglou and Pandis, 2015), myrcene (Hanson et al., 2022) and naphthalene (Chan et al., 2009; He et al., 2022). It is unique to report nucleation rates, or the number of particles produced, as a function of oxidation rate (where here Q_4 is a proxy) for the photo-oxidation of biogenic terpenes.

The present measurements show that β -caryophyllene is more effective than myrcene at producing particles; for equivalent HONO photolysis rates myrcene nucleation was shown to be more effective than sulfuric acid nucleation at 35% relative humidity (Hanson et al., 2022). However, nucleation from photo-oxidation of neither myrcene or β -caryophyllene is expected to be atmospherically



important at room temperature. This is because of the strong dependence of the number of particles on Q_4 (about the fourth power) in **Figure 3** and that our experimental oxidation rates far exceed those in the atmosphere. With the reasonable association of Q_4 and the OH production rate, R_{OH} , N_p goes as roughly R_{OH} to the fourth power. The R_{OH} at the midpoint of the measurements in **Figure 3** is roughly 1,000 times typical mid-day R_{OH} in the atmosphere and the extrapolated N_p produced in the on-axis transit time of ~ 40 s for atmospheric conditions would be 10^{-7} cm^{-3} . Furthermore, β -caryophyllene is quickly lost in the atmosphere by reacting with ozone. For myrcene, however, photo-oxidation of myrcene may play a role in ion-induced nucleation at cold temperatures (Kirkby et al., 2016) or synergistically with sulfuric acid (Riccobono et al., 2014; Kupc et al., 2020).

Mass Spectrometer

A photolysis experiment with ~ 500 ppb α -pinene and 2×10^{12} cm^{-3} HONO was performed with the drift tube voltage for the proton-transfer mass spectrometer operated at about 60% of normal to minimize the breakup of product ions (70 Td). Four mass spectra (each an average of a few spectra with a 1 s dwell at each mass) are shown in **Figure 4**, a plot of signal (linear below 100 Hz, log above that) vs ion mass, 160 to 270 u. Two spectra are with LEDs off and are due to background from α -pinene and/or the system; the second spectra at 17:50 was 3 h after the LEDs were turned off but many species may not have returned fully to background conditions. The orange squares are with the curtain lens raised so that the E/N increased 15–20% in this 0.5 cm long region: this primarily decreased hydration of a few parent M plus proton species, $M.H^+$; for example, one can see

the decreases in the signals at 173 and 191 u which are hydrates of $M\cdot H = 137$ u for α -pinene. Signal at 171 and 189 u also appear to decrease with an increase in this voltage and they appear to be hydrates of 153 u, present as in impurity. Signals decrease at 219 u and 252 u also, and these may be hydrates of 201 u and 234 u, respectively. Most of the peaks in the mass spectra are not affected by this voltage change.

There are a number of significant peaks that arise in **Figure 4** when the LEDs are turned on, notably: pinonaldehyde at 169 u, and two stable species that presumably contain 3 and 4 oxygen atoms at $M\cdot H = 185$ u and 201 u. Identities of these species are not known but, for 201 u, Vereecken et al. (2007) suggested a dicarbonyl ester and 2-OH-8-OOH-menthen-6-one, and for 185 u, a hydroperoxide-ketone, 8-OOH-menthen-6-one. In similar experiments, Lee et al. (2006b) also reported signal at $m/z = 169$ and 185. Our signals result in abundances compared to α -pinene lost of about 60, 7 and 10% for pinonaldehyde, $M\cdot H = 185$ u, and $M\cdot H = 201$ u, respectively, assuming the instrument has the same sensitivities for them as it does for α -pinene (i.e., a signal-based yield, Hanson et al., 2004).

There are many even masses that have signals that are between 0.5 and 1.5% of the change in the α -pinene signal (the signal-based yield). Even mass $M\cdot H^+$ are typically due to radicals or are stable nitrogen containing species. There is a sequence of peaks at 198, 214, 230, 246 that correspond to the $M\cdot H$ of the nitrates (including peroxy nitrates) expected in the OH abstraction pathways from α -pinene (Vereecken et al., 2007; dashed indicators) where several NO molecules have reacted. There is a sequence of peroxy radicals from OH addition to α -pinene with $M = C_{10}H_{17}O_xO_2$, $x = 1$ to 5, with $M\cdot H$ of 186, 202, 218, 234, and 250 u shown in **Figure 4** with the gray indicator lines. The first two are obscured in the signals of the isotopes of 185 u and 201 u while the signal at 234 u is quite prominent. The sequence 216, 232, 248 and 264 u are consistent with the nitrates (including peroxy nitrates) in the OH addition pathways, indicated with red lines. Note that a water of hydration on the 216 u nitrate, if strongly enough bound, could contribute to the signal at 234 u; in general water ligands would complicate the interpretation of the mass spectra. Nonetheless, most of the masses with significant signals in the 214 to 264 u range correspond to $M\cdot H$ masses expected in the photo-oxidation of α -pinene. The three sequences discussed above add up to about an 8% signal-based yield.

The **Supplementary Material** presents more data obtained with the proton-transfer mass spectrometer including a net signal mass spectra of GroFR background with α -pinene present, a time-evolution of some of the product ion signals shown in **Figure 4** and a comparison to the time-evolution of the nanoparticle size measurements. The particle size measurements do not have any decipherable dependence on time during a 45 min LEDs on time period while species that give the 185 u and 201 u ions vary dramatically over the first 45 min of a LEDs on experiment; pinonaldehyde also varies with time rising quickly over the first 10 minutes and then more slowly. Presuming this stickiness is exhibited in GroFR (and quite probably in the mass spectrometer sampling lines etc.) it is hard to see how these species are responsible for α -pinene SOA for our conditions. We plan more targeted experiments in the

future, increasing the seed particle size and number density while monitoring the mass spectra. Researchers with high-resolution PTRMS instrumentation are better suited to ascertain the molecular identities of the α -pinene photo-oxidation products shown in **Figure 4**.

HONO Photolysis Rate

The first-order HONO photolysis rate coefficient, k_{phot} , was estimated in our previous work with GroFR to be 0.002 s^{-1} by comparing modeled H_2SO_4 gas-phase abundance to measured particle growth (Hanson et al., 2022). The gas-kinetic collisional rate coefficient for growth was used with no enhancement due to long-range van der Waals forces.

An alternate assessment of k_{phot} in another of our experiments was done with isoprene photo-oxidation, where k_{phot} was calculated from the increase in the main oxidation products, methylvinylketone and methacrolein, using a simplified kinetic scheme (Hanson et al., 2019). Since then, we have built a detailed 2D model of the photo-oxidation of α -pinene (Hanson et al., 2022) and the amount of impurity NO in the HONO source is now routinely measured. Therefore, we performed three experimental runs with several On-Off cycles of the LEDs to detect with some precision the small change in α -pinene due to photo-oxidation. These measurements are detailed in the **Supplementary Material** and the average k_{phot} is 0.0019 s^{-1} ($\pm 34\%$). This is consistent with our 2022 assessment of k_{phot} obtained from H_2SO_4 growth experiments analyzed without van der Waals enhancements to the gas-kinetic collision rate.

CONCLUSION

This present work surveys how functional groups determine secondary (but first-generation) organic aerosol growth capabilities upon photo-oxidation and for low organic aerosol loadings. Of the groups studied here, cyclic compounds and multi-functional species with an exocyclic C-C double bond generated the largest SOA yields. Exocyclic double bonds lead to peroxy positioning that is better in terms of H-shift rates and overall spacing of oxygenated moieties within the molecule that enhance SOA forming capabilities at small OH exposures. The biogenic C-10 and C-15 compounds studied here are cyclic and possess double bonds, and with the exception of α -pinene, lead to significant growth of seed particles. We find that typical non-functionalized alkanes do not produce significant amounts of SOA material at these OH exposures. The results presented here are consistent with secondary organic aerosol production being dependent on the presence of bidentate oxygenated moieties. So in addition to facile H-shift rates to further gas-phase oxygenation, the adhesion of SOA material to particles is probably influenced by the distribution of the oxygenated moieties on the precursor backbone.

We also presented mass spectrometer measurements of the first-generation photo-oxidation products of α -pinene and determined signal-based yields (or abundances). The results are consistent with large yields of pinonaldehyde (on the order of 50%) and about 10 and 5% of $\text{C}_{10}\text{H}_{16}\text{O}_4$ and

$C_{10}H_{16}O_3$, respectively. The yields for these three species are within reasonable bounds of the predictions of Vereecken et al. (2007). The time evolution of these product ions are disconnected from changes in the particle sizes which were immediate upon initiation of photo-oxidation; either the products that were detected do not contribute to SOA or their interactions with the walls does not influence their uptake onto particles.

We observed several sequences of even mass ions that are consistent with multifunctional nitrates and peroxy radicals formed in α -pinene photo-oxidation schemes; the sum of these signals led to a yield of about 8%. An ion at mass 234 had the largest signal of all the ions from 205 to 270 u and it is consistent with $M\cdot H^+$ of an OH-addition channel RO_6 peroxy radical, however, it is also consistent with an H_2O ligand on $M\cdot H^+$ of an OH-addition channel hydroxyl nitrate. The calibration of the mass spectrometer for α -pinene, measured HONO level, and the amount of α -pinene lost upon photooxidation allowed for a determination of the photolysis rate for HONO of 0.0019 s^{-1} (but with an uncertainty of 34%). This is in good agreement with that derived from H_2SO_4 growth considerations without van der Waals effects in our previous work (Hanson et al., 2022).

The SOA results are relevant to the atmosphere because small sulfuric acid seed particles are representative of some portion of the nucleation mode aerosol and their growth is critically important in climate processes. The atmospheric relevance is also through understanding the initial SOA capabilities of organic compounds undergoing photo-oxidation. For example,

understanding the role of functional groups will aid SOA incorporation into atmospheric models. Discovering the reasons for the observed linear increases with photo-oxidation rate may uncover new first-generation chemical pathways important for atmospheric conditions. The work presented here is a unique way to study organic aerosol formation, providing a challenge to SOA modeling efforts.

DATA AVAILABILITY STATEMENT

The raw data supporting the conclusions of this article will be made available by the authors, without undue reservation.

AUTHOR CONTRIBUTIONS

DS and DL conducted the experiments and analyzed the data, TK contributed modeling efforts, DH, MW and JK provided guidance and helped with the analysis, and DS and DH wrote the manuscript.

SUPPLEMENTARY MATERIAL

The Supplementary Material for this article can be found online at: <https://www.frontiersin.org/articles/10.3389/fenvs.2022.892389/full#supplementary-material>

REFERENCES

- Alfarra, M. R., Hamilton, J. F., Wyche, K. P., Good, N., Ward, M. W., Carr, T., et al. (2012). The Effect of Photochemical Ageing and Initial Precursor Concentration on the Composition and Hygroscopic Properties of B-Caryophyllene Secondary Organic Aerosol. *Atmos. Chem. Phys.* 12, 6417–6436. doi:10.5194/acp-12-6417-2012
- Berndt, T., Richters, S., Jokinen, T., Hyttinen, N., Kurtén, T., Otkjær, R. V., et al. (2016). Hydroxyl Radical-Induced Formation of Highly Oxidized Organic Compounds. *Nat. Commun.* 7, 13677. doi:10.1038/ncomms13677
- Chan, A. W. H., Kautzman, K. E., Chhabra, P. S., Surratt, J. D., Chan, M. N., Crouse, J. D., et al. (2009). Secondary Organic Aerosol Formation from Photooxidation of Naphthalene and Alkyl-naphthalenes: Implications for Oxidation of Intermediate Volatility Organic Compounds (IVOCs). *Atmos. Chem. Phys.* 9, 3049–3060. doi:10.5194/acp-9-3049-2009
- Chan, M. N., Surratt, J. D., Chan, A. W. H., Schilling, K., Offenberg, J. H., Lewandowski, M., et al. (2011). Influence of Aerosol Acidity on the Chemical Composition of Secondary Organic Aerosol from β -caryophyllene. *Atmos. Chem. Phys.* 11, 1735–1751. doi:10.5194/acp-11-1735-2011
- Chiappini, L., Perraudin, E., Maurin, N., Picquet-Varrault, B., Zheng, W., Marchand, N., et al. (2019). Secondary Organic Aerosol Formation from Aromatic Alkane Ozonolysis: Influence of the Precursor Structure on Yield, Chemical Composition, and Mechanism. *J. Phys. Chem. A* 123, 1469–1484. doi:10.1021/acs.jpca.8b10394
- Donahue, N. M., Epstein, S. A., Pandis, S. N., and Robinson, A. L. (2011). A Two-Dimensional Volatility Basis Set: 1. Organic-Aerosol Mixing Thermodynamics. *Atmos. Chem. Phys.* 11, 3303–3318. doi:10.5194/acp-11-3303-2011
- Febo, A., Perrino, C., Gherardi, M., and Sparapani, R. (1995). Evaluation of a High-Purity and High-Stability Continuous Generation System for Nitrous Acid. *Environ. Sci. Technol.* 29, 2390–2395. doi:10.1021/es00009a035
- Gingerysty, N. J., and Osthoff, H. D. (2020). A Compact, High-Purity Source of HONO Validated by Fourier Transform Infrared and Thermal-dissociation Cavity Ring-Down Spectroscopy. *Atmos. Meas. Tech.* 13, 4159–4167. doi:10.5194/amt-13-4159-2020
- Hanson, D., Orlando, J., Noziere, B., and Kosciuch, E. (2004). Proton Transfer Mass Spectrometry Studies of Peroxy Radicals. *Int. J. Mass Spectrom.* 239, 147–159. doi:10.1016/j.ijms.2004.07.021
- Hanson, D. R., and Eisele, F. (2000). Diffusion of H_2SO_4 in Humidified Nitrogen: Hydrated H_2SO_4 . *J. Phys. Chem. A* 104, 1715–1719. doi:10.1021/jp993622j
- Hanson, D. R., Koppes, M., Stoffers, A., Harsdorf, R., and Edelen, K. (2009). Proton Transfer Mass Spectrometry at 11hPa with a Circular Glow Discharge: Sensitivities and Applications. *Int. J. Mass Spectrom.* 282, 28–37. doi:10.1016/j.ijms.2009.01.021
- Hanson, D. R., Abdullahi, H., Menheer, S., Vences, M. R., Alves, M., and Kunz, J. (2019). H_2SO_4 and Particle Production in a Photolytic Flow Reactor: Chemical Modeling, Cluster Thermodynamics and Contamination Issues. *Atmos. Chem. Phys.* 19, 8999–9015. doi:10.5194/acp-19-8999-2019
- Hanson, D. R., Sawyer, A., Long, D., Sofio, D., Kunz, J., and Wentzel, M. (2022). Particle Formation from Photooxidation of α -pinene, Limonene, and Myrcene. *J. Phys. Chem. A* 126, 910–923. doi:10.1021/acs.jpca.1c08427
- Haywood, J., and Boucher, O. (2000). Estimates of the Direct and Indirect Radiative Forcing Due to Tropospheric Aerosols: A Review. *Rev. Geophys.* 38, 513–543. doi:10.1029/1999RG000078
- He, Q., Li, C., Siemens, K., Morales, A. C., Hettiyadura, A. P. S., Laskin, A., et al. (2022). Optical Properties of Secondary Organic Aerosol Produced by Photooxidation of Naphthalene under NOx Condition. *Environ. Sci. Technol.* 56 (8), 4816–4827. doi:10.1021/acs.est.1c07328
- Hunter, J. F., Carrasquillo, A. J., Daumit, K. E., and Kroll, J. H. (2014). Secondary Organic Aerosol Formation from Acyclic, Monocyclic, and Polycyclic Alkanes. *Environ. Sci. Technol.* 48, 10227–10234. doi:10.1021/es502674s

- Jiang, J., Chen, M., Kuang, C., Attoui, M., and McMurry, P. H. (2011). Electrical Mobility Spectrometer Using a Diethylene Glycol Condensation Particle Counter for Measurement of Aerosol Size Distributions Down to 1 Nm. *Aerosol Sci. Technol.* 45, 510–521. doi:10.1080/02786826.2010.547538
- Jimenez, J. L., Canagaratna, M. R., Donahue, N. M., Prevot, A. S. H., Zhang, Q., Kroll, J. H., et al. (2009). Evolution of Organic Aerosols in the Atmosphere. *Science* 326, 1525–1529. doi:10.1126/science.1180353
- Keywood, M. D., Varutbangkul, V., Bahreini, R., Flagan, R. C., and Seinfeld, J. H. (2004). Secondary Organic Aerosol Formation from the Ozonolysis of Cycloalkenes and Related Compounds. *Environ. Sci. Technol.* 38, 4157–4164. doi:10.1021/es035363o
- Kirkby, J., Duplissy, J., Sengupta, K., Frege, C., Gordon, H., Williamson, C., et al. (2016). Ion-induced Nucleation of Pure Biogenic Particles. *Nature* 533, 521–526. doi:10.1038/nature17953
- Krasnomowitz, J. M., Apsokardu, M. J., Stangl, C. M., Tiszenkel, L., Ouyang, Q., Lee, S., et al. (2019). Growth of Aitken Mode Ammonium Sulfate Particles by α -pinene Ozonolysis. *Aerosol Sci. Technol.* 53, 406–418. doi:10.1080/02786826.2019.1568381
- Kroll, J. H., and Seinfeld, J. H. (2008). Chemistry of Secondary Organic Aerosol: Formation and Evolution of Low-Volatility Organics in the Atmosphere. *Atmos. Environ.* 42, 3593–3624. doi:10.1016/j.atmosenv.2008.01.003
- Kupc, A., Williamson, C. J., Hodshire, A. L., Kazil, J., Ray, E., Bui, T. P., et al. (2020). The Potential Role of Organics in New Particle Formation and Initial Growth in the Remote Tropical Upper Troposphere. *Atmos. Chem. Phys.* 20, 15037–15060. doi:10.5194/acp-20-15037-2020
- Lee, A., Goldstein, A. H., Keywood, M. D., Gao, S., Varutbangkul, V., Bahreini, R., et al. (2006a). Gas-phase Products and Secondary Aerosol Yields from the Ozonolysis of Ten Different Terpenes. *J. Geophys. Res.* 111, D07302. doi:10.1029/2005JD006437
- Lee, A., Goldstein, A. H., Kroll, J. H., Ng, N. L., Varutbangkul, V., Flagan, R. C., et al. (2006b). Gas-phase Products and Secondary Aerosol Yields from the Photooxidation of 16 Different Terpenes. *J. Geophys. Res.* 111, D17305. doi:10.1029/2006JD007050
- Lee, S. H., Gordon, H., Yu, H., Lehtipalo, K., Haley, R., Li, Y., et al. (2019). New Particle Formation in the Atmosphere: From Molecular Clusters to Global Climate. *J. Geophys. Res. Atmos.* 124, 7098–7146. doi:10.1029/2018JD029356
- Li, J., Li, H., Li, K., Chen, Y., Zhang, H., Zhang, X., et al. (2021). Enhanced Secondary Organic Aerosol Formation from the Photo-Oxidation of Mixed Anthropogenic Volatile Organic Compounds. *Atmos. Chem. Phys.* 21, 7773–7789. doi:10.5194/acp-21-7773-2021
- Li, K., Liggio, J., Lee, P., Han, C., Liu, Q., and Li, S.-M. (2019). Secondary Organic Aerosol Formation from α -pinene, Alkanes, and Oil-Sands-Related Precursors in a New Oxidation Flow Reactor. *Atmos. Chem. Phys.* 19, 9715–9731. doi:10.5194/acp-19-9715-2019
- Lim, Y. B., and Ziemann, P. J. (2009). Effects of Molecular Structure on Aerosol Yields from OH Radical-Initiated Reactions of Linear, Branched, and Cyclic Alkanes in the Presence of NO_x . *Environ. Sci. Technol.* 43, 2328–2334. doi:10.1021/es803389s
- Møller, K. H., Otkjær, R. V., Chen, J., and Kjaergaard, H. G. (2020). Double Bonds Are Key to Fast Unimolecular Reactivity in First-Generation Monoterpene Hydroxy Peroxy Radicals. *J. Phys. Chem. A* 124, 2885–2896. doi:10.1021/acs.jpca.0c01079
- Ng, N. L., Kroll, J. H., Keywood, M. D., Bahreini, R., Varutbangkul, V., Flagan, R. C., et al. (2006). Contribution of First- versus Second-Generation Products to Secondary Organic Aerosols Formed in the Oxidation of Biogenic Hydrocarbons. *Environ. Sci. Technol.* 40, 2283–2297. doi:10.1021/es052269u
- Praske, E., Otkjær, R. V., Crounse, J. D., Hethcox, J. C., Stoltz, B. M., Kjaergaard, H. G., et al. (2018). Atmospheric Autoxidation Is Increasingly Important in Urban and Suburban North America. *Proc. Natl. Acad. Sci. U.S.A.* 115, 64–69. doi:10.1073/pnas.1715540115
- Raventos-Duran, T., Camredon, M., Valorso, R., Mouchel-Vallon, C., and Aumont, B. (2010). Structure-activity Relationships to Estimate the Effective Henry's Law Constants of Organics of Atmospheric Interest. *Atmos. Chem. Phys.* 10, 7643–7654. doi:10.5194/acp-10-7643-2010
- Riccobono, F., Schobesberger, S., Scott, C. E., Dommen, J., Ortega, I. K., Rondo, L., et al. (2014). Oxidation Products of Biogenic Emissions Contribute to Nucleation of Atmospheric Particles. *Science* 344, 717–721. doi:10.1126/science.1243527
- Sato, K., Takami, A., Kato, Y., Seta, T., Fujitani, Y., Hikida, T., et al. (2012). AMS and LC/MS Analyses of SOA from the Photooxidation of Benzene and 1,3,5-trimethylbenzene in the Presence of NO_x : Effects of Chemical Structure on SOA Aging. *Atmos. Chem. Phys.* 12, 4667–4682. doi:10.5194/acp-12-4667-2012
- Tasoglou, A., and Pandis, S. N. (2015). Formation and Chemical Aging of Secondary Organic Aerosol during the β -caryophyllene Oxidation. *Atmos. Chem. Phys.* 15, 6035–6046. doi:10.5194/acp-15-6035-2015
- Tkacik, D. S., Presto, A. A., Donahue, N. M., and Robinson, A. L. (2012). Secondary Organic Aerosol Formation from Intermediate-Volatility Organic Compounds: Cyclic, Linear, and Branched Alkanes. *Environ. Sci. Technol.* 46, 8773–8781. doi:10.1021/es301112c
- Tuet, W. Y., Chen, Y., Fok, S., Champion, J. A., and Ng, N. L. (2017). Inflammatory Responses to Secondary Organic Aerosols (SOA) Generated from Biogenic and Anthropogenic Precursors. *Atmos. Chem. Phys.* 17, 11423–11440. doi:10.5194/acp-17-11423-2017
- Vereecken, L., Müller, J.-F., and Peeters, J. (2007). Low-volatility Poly-Oxygenates in the OH-initiated Atmospheric Oxidation of α -pinene: Impact of Non-traditional Peroxyl Radical Chemistry. *Phys. Chem. Chem. Phys.* 9, 5241. doi:10.1039/b708023a
- Vereecken, L., and Nozière, B. (2020). H Migration in Peroxy Radicals under Atmospheric Conditions. *Atmos. Chem. Phys.* 20, 7429–7458. doi:10.5194/acp-20-7429-2020
- Vereecken, L., and Peeters, J. (2012). A Theoretical Study of the OH-initiated Gas-phase Oxidation Mechanism of β -Pinene (C₁₀H₁₆): First Generation Products. *Phys. Chem. Chem. Phys.* 14, 3802. doi:10.1039/c2cp23711c
- Xu, L., Møller, K. H., Crounse, J. D., Otkjær, R. V., Kjaergaard, H. G., and Wennberg, P. O. (2019). Unimolecular Reactions of Peroxy Radicals Formed in the Oxidation of α -Pinene and β -Pinene by Hydroxyl Radicals. *J. Phys. Chem. A* 123, 1661–1674. doi:10.1021/acs.jpca.8b11726
- Zhao, D. F., Kaminski, M., Schlag, P., Fuchs, H., Acir, I.-H., Bohn, B., et al. (2015). Secondary Organic Aerosol Formation from Hydroxyl Radical Oxidation and Ozonolysis of Monoterpenes. *Atmos. Chem. Phys.* 15, 991–1012. doi:10.5194/acp-15-991-2015
- Zhu, J., Penner, J. E., Lin, G., Zhou, C., Xu, L., and Zhuang, B. (2017). Mechanism of SOA Formation Determines Magnitude of Radiative Effects. *Proc. Natl. Acad. Sci. U.S.A.* 114, 12685–12690. doi:10.1073/pnas.1712273114

Conflict of Interest: The authors declare that the research was conducted in the absence of any commercial or financial relationships that could be construed as a potential conflict of interest.

Publisher's Note: All claims expressed in this article are solely those of the authors and do not necessarily represent those of their affiliated organizations, or those of the publisher, the editors and the reviewers. Any product that may be evaluated in this article, or claim that may be made by its manufacturer, is not guaranteed or endorsed by the publisher.

Copyright © 2022 Sofio, Long, Kohls, Kunz, Wentzel and Hanson. This is an open-access article distributed under the terms of the Creative Commons Attribution License (CC BY). The use, distribution or reproduction in other forums is permitted, provided the original author(s) and the copyright owner(s) are credited and that the original publication in this journal is cited, in accordance with accepted academic practice. No use, distribution or reproduction is permitted which does not comply with these terms.